Chem. Mater. **2008,** *20,* 5807–5815

Nanoparticle Precursors and Phase Selectivity in Hydrothermal Synthesis of Zeolite β

Nathan D. Hould and Raul F. Lobo*

Center for Catalytic Science and Technology, Department of Chemical Engineering, University of Delaware, Newark, Delaware 19716

Received March 27, 2008. Revised Manuscript Received June 23, 2008

The crystallization mechanism of zeolite β in relatively dilute solutions composed of $1SiO_2/80H_2O/0.25TEA_2O/4EtOH/(0.05 + Y)Na_2O/YAl_2O_3/WB_2O_3$, where Y is 0 and 0.01 and W is 0 and 0.025, was investigated using small-angle X-ray scattering, dynamic light scattering, X-ray diffraction, and electron microscopy. In this system there is a critical aggregation concentration (cac) for silica above which silica monomers and oligomers aggregate into primary nanoparticles (<3 nm), and there is an inverse correlation between the cac and the boric acid concentration. When these solutions are heated (120 °C) some of the primary particles transform into larger secondary particles (6−50 nm). In solutions without aluminum the secondary particles remain stable for extended periods of time. In solutions with aluminum the secondary particles aggregate into tertiary particles (zeolite β, >200 nm). The tertiary particles initially have poor long-range order and an oblate morphology. They evolve into zeolite β crystals with longer-range order, a smoother surface, and a square bipyramidal morphology by solution-mediated silica reorganization.

1. Introduction

High-silica zeolites are commonly synthesized in aqueous solutions or gels that contain a silica source, a cationic structure-directing agent (SDA), and hydroxide ions at high temperatures (>373 K) and autogenous pressure.[1−3] A wide range of crystalline architectures and acid site densities and strengths are possible in the resulting solid by changing the geometry and chemical properties (organic or inorganic) of the SDA and by adding heteroatoms into the synthesis mixture (Al, B, Ge, etc.).[4−6] Despite the success of the zeolite community in preparing new frameworks in the last 2 decades, a detailed understanding of how zeolite nucleation and growth are connected to the initial solution composition at the molecular level is lacking. Therefore, the design of new zeolites requires extensive effort to test feasible syntheses using trial and error.

One obstacle to a fundamental understanding of the molecular events in zeolite formation is that many in situ techniques are inapplicable to hydrothermal syntheses because of the high temperatures and pressures employed. Another complication is the compositions used in standard zeolite syntheses (highly concentrated). These difficulties prompted research on silicalite-1, the purely siliceous form of ZSM-5, in "clear solutions" at relatively low temperatures (<373 K).[7−12] The transparent nature of these solutions facilitates the use of in situ light and X-ray scattering techniques, and because they are composed of only tetraethyl orthosilicate (TEOS), tetrapropyl ammonium (TPA) hydroxide, and water they are compositionally simple.

In these clear solutions there is a critical aggregation concentration (cac) above which monomeric and oligomeric silica self-assemble into small colloidal nanoparticles (<5 nm).[10,13−15] The role that these nanoparticles play in the formation of silicalite-1 is the subject of many reports. In the model proposed by Davis et al.[16] precursor nanoparticles (PN) with a core of amorphous silica and a shell of TPA[13] are formed above the cac. Over time the PN become more ordered (higher connectivity),[17] and some of them serve as silicalite-1 nuclei that aggregate with other "intermediate" nanoparticle species to form larger silicalite-1 crystals. In this model Derjaguin−Landau−Verwey−Overbeek (DLVO)

---

* Corresponding author. E-mail: lobo@udel.edu. Tel.: 302-831-1261. Fax: 302-831-1048.

(1) Auerbach, S. M.; Carrado, K. A.; Dutta, P. K. *Handbook of Zeolite Science and Technology*; Marcel Dekker: New York, 2003.
(2) Breck, D. W. *Zeolite Molecular Sieves*; Wiley: London, 1982.
(3) Tanabe, K.; Holderich, W. F. *Appl. Catal., A* **1999**, *181* (2), 399–434.
(4) Chu, C. T. W.; Chang, C. D. *J. Phys. Chem.* **1985**, *89* (9), 1569–1571.
(5) Gies, H.; Marker, B. *Zeolites* **1992**, *12* (1), 42–49.
(6) Zones, S. I.; Davis, M. E. *Curr. Opin. Solid State Mater. Sci.* **1996**, *1* (1), 107–117.
(7) Pelster, S. A.; Schrader, W.; Schuth, F. *J. Am. Chem. Soc.* **2006**, *128* (13), 4310–4317.
(8) Kragten, D. D.; Fedeyko, J. M.; Sawant, K. R.; Rimer, J. D.; Vlachos, D. G.; Lobo, R. F.; Tsapatsis, M. *J. Phys. Chem. B* **2003**, *107* (37), 10006–10016.
(9) Fedeyko, J. M.; Vlachos, D. G.; Lobo, R. F. *Langmuir* **2005**, *21* (11), 5197–5206.
(10) Schoeman, B. J. *Zeolites* **1997**, *18* (2−3), 97–105.
(11) Yang, S.; Navrotsky, A. *Chem. Mater.* **2002**, *14* (6), 2803–2811.
(12) Patis, A.; Dracopoulos, V.; Nikolakis, V. *J. Phys. Chem. C* **2007**, *111* (47), 17478–17484.
(13) Fedeyko, J. M.; Rimer, J. D.; Lobo, R. F.; Vlachos, D. G. *J. Phys. Chem. B* **2004**, *108* (33), 12271–12275.
(14) Rimer, J. D.; Fedeyko, J. M.; Vlachos, D. G.; Lobo, R. F. *Chem.—Eur. J.* **2006**, *12* (11), 2926–2934.
(15) Rimer, J. D.; Lobo, R. F.; Vlachos, D. G. *Langmuir* **2005**, *21* (19), 8960–8971.
(16) Davis, T. M.; Drews, T. O.; Ramanan, H.; He, C.; Dong, J. S.; Schnablegger, H.; Katsoulakis, M. A.; Kokkoli, E.; McCormick, A. V.; Penn, R. L.; Tsapatsis, M. *Nat. Mater.* **2006**, *5* (5), 400–408.
(17) Provis, J. L.; Gehman, J. D.; White, C. E.; Vlachos, D. G. *J. Phys. Chem. C* **2008**.

10.1021/cm800884q CCC: $40.75

theory is used to calculate rates of nanoparticle−crystal aggregation.[16,18,19] Other models propose that the formation of silicalite-1 occurs by oriented aggregation of precursors, all of which have the structure of silicalite-1.[20−23]

Although the majority of studies related to zeolite formation focus on silicalite-1, studies of clear solutions using SDAs that yield ZSM-12, ZSM-11, zeolite β, and Linde type A zeolite are noteworthy.[24−28] Throughout these studies there has been little emphasis on the effects that trivalent heteroatoms (Al, B) have on zeolite formation. These elements are important because of the role that these framework substitutions have played in the discovery of new zeolites and because they give rise to their remarkable catalytic properties.[6,29]

Zeolite β is particularly interesting because it can be synthesized over a wide range of Si to Al ratios (from 5 to ∞)[24,30] and because it is used industrially to produce cumene.[3] It is synthesized in solutions similar in composition to those used to make silicalite-1, except that tetraethylammonium (TEA) is the SDA.[31] In dilute aqueous solutions of TEAOH and TEOS silica self-assembles into PNs with a silica core and SDA shell similar to those formed in clear solution silicalite-1 syntheses.[13] Mintova et al. have synthesized nanocrystals of zeolite β with varying Si to Al ratios.[32] They detected a bimodal distribution of particles (precursors and crystals) in solution and found a direct correlation between aluminum concentration in the synthesis solution and the rate of zeolite β formation. Also, a mesoporous silica with zeolite β micropores has been synthesized by adding a triblock copolymer ($PEO_{20}-PPO_{70}-PEO_{20}$) to a solution of zeolite β precursor particles.[33,34] This material, named MAS-7, is notable because it has the reactivity and thermal stability of zeolite β but is not subject to the same diffusion limitations as conventional microporous materials.

Table 1

name	Si/Al	Si/B	zeolite product
Z1	50	20	β
Z2	50	∞	β
Z3	∞	20	none
Z4	∞	∞	none

The mechanism of zeolite β formation in relatively dilute solutions is investigated in this report using dynamic light scattering (DLS), small-angle X-ray scattering (SAXS), high-resolution electron microscopy (HREM), and X-ray diffraction (XRD). In solutions containing aluminum three populations of particles are observed when this solution is heated at 120 °C: primary particles (<3 nm), secondary particles (6−50 nm), and tertiary particles (zeolite β, > 200 nm). Solutions without aluminum do not form tertiary particles, and the tertiary particles are aggregates of secondary particles some of which have zeolite β crystal structure. The morphology and crystallinity of tertiary particles improve over time by solution-mediated silica reorganization.

2. Experimental Section

2.1. Synthesis. *2.1.1. Nanoparticles.* Solutions of molar composition $X SiO_2/9500H_2O/20TEA_2O/4X EtOH/W B_2O_3$ where X and W vary from 0 to 60, and 0 to 2, respectively, were prepared in two steps. In the first step TEAOH (35% w/w, Alfa Aesar) and boric acid (≥99.5%, Sigma-Aldrich) are added to deionized (DI) water and stirred for approximately 30 min. In the second step TEOS (98%, Aldrich) is added to this mixture, and the resulting clear solution is stirred for at least 12 h to complete hydrolysis. Selected samples ($X = 40$, $W = 0$ or 2) are loaded into 15 mL polypropylene tubes and submerged in a mineral oil bath maintained at 80 °C. These samples are quenched to room temperature before characterization.

2.1.2. Zeolite β. Solutions of molar composition $1SiO_2/80H_2O/0.25TEA_2O/4EtOH/(0.05 + Y)Na_2O/Y Al_2O_3/W B_2O_3$ where Y is 0 and 0.01 and W is 0 and 0.025 were investigated (Table 1).[31] TEOS is hydrolyzed in a solution containing 10% of the DI water and all of the TEAOH solution. After hydrolysis is complete (~2 h) a homogeneous solution with the remaining components (NaOH, $NaAlO_2$, and $B(OH)_3$) and water is added into the first solution under stirring. The resulting clear solution is stirred for about 1 h and is then loaded into a PTFE acid digestion vessel (120 mL, Savillex) sealed with PTFE tape. The bomb is placed in a convection oven and heated at 120 °C under static conditions. Bombs are quenched to room temperature after various heating times for characterization. Solids are removed by centrifugation at approximately 3000*g* and dried overnight at 80 °C.

2.2. Analytical Methods. The conductivity of the solutions was measured with a VWR scientific model 2052 EC meter. The hydroxide concentrations (pH) were determined using a Corning 355 pH/ion analyzer equipped with an Orion Ross electrode (model 8104). Before collecting pH data the meter was calibrated using pH 10 and 12 standard buffer solutions. ^{11}B nuclear magnetic resonance (NMR) spectra were collected on a Bruker AV400 spectrometer operating at 128.39 MHz using a routine single-pulse program and 5 mm thin-walled quartz NMR tubes (Willmad LabGlass). A backward linear prediction is used to remove background signal. All samples were diluted 1 time by volume with D_2O, and the part-per-million (ppm) scale is fixed with the D_2O lock.

SAXS patterns were collected on a SAXSess instrument (Anton-Paar) using line-collimated Cu Kα radiation (1.542 Å) and a

---

(18) Nikolakis, V.; Kokkoli, E.; Tirrell, M.; Tsapatsis, M.; Vlachos, D. G. *Chem. Mater.* **2000**, *12* (3), 845–853.
(19) Drews, T. O.; Tsapatsis, M. *Microporous Mesoporous Mater.* **2007**, *101* (1−2), 97–107.
(20) Kirschhock, C. E. A.; Buschmann, V.; Kremer, S.; Ravishankar, R.; Houssin, C. J. Y.; Mojet, B. L.; van Santen, R. A.; Grobet, P. J.; Jacobs, P. A.; Martens, J. A. *Angew. Chem., Int. Ed.* **2001**, *40* (14), 2637–2640.
(21) Kirschhock, C. E. A.; Kremer, S. P. B.; Grobet, P. J.; Jacobs, P. A.; Martens, J. A. *J. Phys. Chem. B* **2002**, *106* (19), 4897–4900.
(22) Kirschhock, C. E. A.; Ravishankar, R.; Jacobs, P. A.; Martens, J. A. *J. Phys. Chem. B* **1999**, *103* (50), 11021–11027.
(23) Kirschhock, C. E. A.; Ravishankar, R.; Looveren, L. V.; Jacobs, P. A.; Martens, J. A. *J. Phys. Chem. B* **1999**, *103* (24), 4972–4978.
(24) de Moor, P.; Beelen, T. P. M.; van Santen, R. A.; Tsuji, K.; Davis, M. E. *Chem. Mater.* **1999**, *11* (1), 36–43.
(25) Cheng, C. H.; Shantz, D. F. *J. Phys. Chem. B* **2005**, *109* (15), 7266–7274.
(26) Fan, W.; Ogura, M.; Sankar, G.; Okubo, T. *Chem. Mater.* **2007**, *19* (8), 1906–1917.
(27) Fan, W.; Meneau, F.; Bras, W.; Ogura, M.; Sankar, G.; Okubo, T. *Microporous Mesoporous Mater.* **2007**, *101* (1−2), 134–141.
(28) Pelster, S. A.; Kalamajka, R.; Schrader, W.; Schüth, F. *Angew. Chem., Int. Ed.* **2007**, *46* (13), 2299–2302.
(29) Burton, A. W.; Zones, S. I.; Elomari, S. *Curr. Opin. Colloid Interface Sci.* **2005**, *10* (5−6), 211–219.
(30) Borade, R. B.; Clearfield, A. *Microporous Mater.* **1996**, *5* (5), 289–297.
(31) de Ruiter, R.; Pamin, K.; Kentgens, A. P. M.; Jansen, J. C.; Vanbekkum, H. *Zeolites* **1993**, *13* (8), 611–621.
(32) Mintova, S.; Valtchev, V.; Onfroy, T.; Marichal, C.; Knozinger, H.; Bein, T. *Microporous Mesoporous Mater.* **2006**, *90* (1−3), 237–245.
(33) Liu, J.; Zhang, X.; Han, Y.; Xiao, F. S. *Chem. Mater.* **2002**, *14* (6), 2536–2540.
(34) Han, Y.; Xiao, F. S.; Wu, S.; Sun, Y.; Meng, X.; Li, D.; Lin, S.; Deng, F.; Ai, X. *J. Phys. Chem. B* **2001**, *105* (33), 7963–7966.

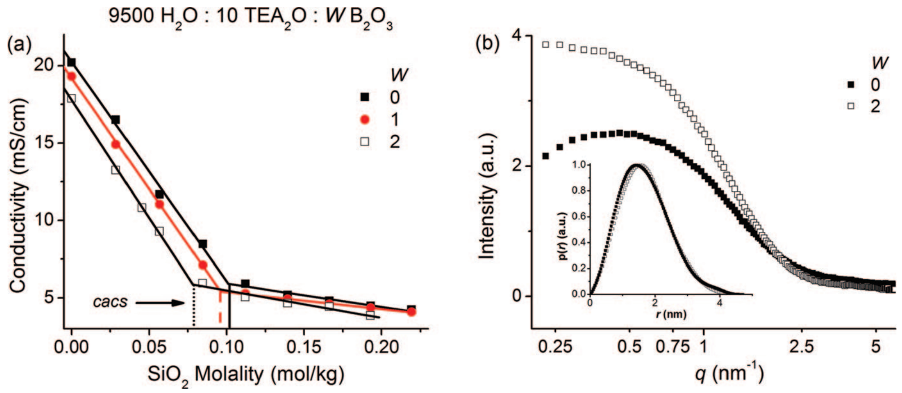

Figure 1. (a) Plots of conductivity with increasing silica concentration. The points are experimental data, and the lines are fits used to calculate the cacs. Drop lines are placed on the cacs for clarity. (b) SAXS patterns from nanoparticles self-assembled in solutions composed of $40SiO_2/9500H_2O/20TEAOH/ZB(OH)_3$. The inset shows the PDDFs (scaled to $p_{max} = 1$) of the two SAXS patterns.

phosphor image plate. The sample holder is a TCS120 (Anton-Paar) that is fitted for liquid samples in a quartz capillary (1 mm diameter). The q-scale is determined relative to the maximum intensity of the primary attenuated beam ($q = 0$) which is subsequently used to scale the intensity of the scattering pattern ($I(q = 0) = 1$). Afterward a water background is subtracted from the scattering pattern. The scattering intensity is then placed on an absolute scale using the method developed by Orthaber et al.[35] In our protocol the scattering intensity of water at zero scattering angle ($I(q = 0)$) is estimated by averaging the scattering intensity over the q-range from 2 to 5 nm^{-1}.

After scaling the intensity real-space information is obtained using pair distance distribution functions (PDDFs) calculated with the indirect Fourier transform (IFT) technique.[36,37] The IFT technique is advantageous because it requires minimal a priori information about the particles contributing to the scattering pattern. Only an upper limit to the particle size must be input into the algorithm to acquire real-space information about the particles. It also simultaneously employs a desmearing routine that calculates the ideal pinhole-collimated scattering intensity from the experimental scattering intensity and the beam geometry.[36,38] In some cases we used model direct approaches to the solution of SAXS patterns. In these cases the algorithm reported by Lake[39] is used to desmear the data before they are least-squares fit to various models in a software package developed at the National Center for Neutron Research.[40]

Light scattering data were collected using a BI9000AT correlator and a BI200SM goniometer (Brookhaven Instruments). A model 95 argon ion laser (Lexel Laser) operating at a wavelength of 488 nm is used as a light source. DLS data are collected at a scattering angle of 90°, and each spectrum is measured for 10 min. Generally six spectra are collected for each sample. Brookhaven instruments software is used to calculate the electric field autocorrelation function, and the line width distribution function is calculated using Provencher's integral inversion routine (CONTIN).[41,42] Hydrodynamic size distributions are calculated from the line width distribution using the Stokes–Einstein equation under the assumptions that the particles are spherical and that the solution viscosity is that of water. The calculated particles size distributions for each sample are normalized and then averaged. Samples are clarified using 800 and 2000 nm syringe filters, and those that are too turbid for DLS investigation are diluted from 1 to 11 g with DI water before measurements are performed.

Powder XRD data were collected with a Philips X'Pert X-ray diffractometer equipped with a source of Cu Kα radiation. Scattering intensity is measured from 5° to 50° 2θ in 0.02° steps at 3 s per step. HREM imaging was performed using a JEOL 2010 F transmission electron microscope (TEM) operated at 200 keV. The TEM was equipped with a Schottky field emission gun with a 0.9 eV energy spread and a 1.9 A objective pole piece having a useful resolution limit of 1.3 Å (JEOL). A Gatan 1024 × 1024 CCD camera was used to capture HREM images. The scanning electron microscope (SEM) images were collected on a JEOL 7400F equipped with a field emission gun, capable of 1.5 nm resolution. The laser-enhanced ionization (LEI) detector is operated between 2.0 and 3.0 keV using working distances between 7.5 and 8.5 mm.

3. Results

3.1. Self-Assembly of Silica Nanoparticles. To determine if boron is sequestered into the silica nanoparticles we studied its effect on the cac. These data (Figure 1a and Figure S1 in the Supporting Information) are in agreement with values reported by Fedeyko and co-workers[9,13] and indicate an indirect relationship between the cac and the molality of boric acid.

In solution the distribution of boric acid and its conjugate base (borate) is governed by the following equilibrium with a pK_a of 9.235.[43]

$$B(OH)_3 + H_2O \leftrightarrow B(OH)_4^- + H^+ \qquad (1)$$

Over the pH range studied boric acid exists predominantly as its conjugate base where it is a sink for hydroxide ions. Thus, the effect of boric acid on these solutions is to decrease the pH. Previous reports show a direct relationship between the initial hydroxide concentration and the cac of silica.[9] Because we observed a similar trend, we conclude that boric acid is a spectator ion in nanoparticle self-assembly. It affects the cac indirectly by modifying the pH, and it does not polymerize with the silicate species. This is in agreement

---

(35) Orthaber, D.; Bergmann, A.; Glatter, O. *J. Appl. Crystallogr.* **2000**, *33*, 218–225.
(36) Glatter, O. *J. Appl. Crystallogr.* **1977**, *10*, 415–421.
(37) Pedersen, J. S. *Adv. Colloid Interface Sci.* **1997**, *70*, 171–210.
(38) Glatter, O.; Kratky, O. *Small Angle X-ray Scattering*; Academic Press: New York, 1982.
(39) Lake, J. A. *Acta Crystallogr.* **1967**, *23*, 191–194.
(40) Kline, S. R. *J. Appl. Crystallogr.* **2006**, *39*, 895–900.
(41) Provencher, S. W. *Comput. Phys. Commun.* **1982**, *27* (3), 213–227.
(42) Provencher, S. W. *Comput. Phys. Commun.* **1982**, *27* (3), 229–242.
(43) Baes, C. F., Jr.; Mesmer, R. E. *The Hydrolysis of Cations*; John Wiley & Sons: New York, 1976.

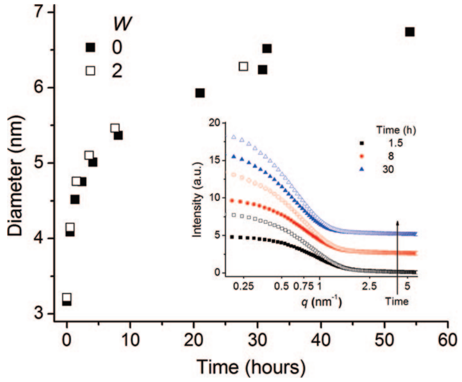

Figure 2. Nanoparticle diameters determined by modeling the PDDFs as monodisperse spheres. The inset shows the evolution of the smeared SAXS patterns over time. Intensity offsets in the inset are 2.5.

with reports of the low affinity that boron has for forming oligomers with silica.[44,45]

This result can be compared to silica nanoparticles formed in the presence of more strongly silica binding species like aluminum.[46] In these systems there is a direct relationship between the cac and the aluminum concentration. Nanoparticles formed in these systems with TPA also have a smaller size that was attributed to electrostatic repulsion from charged aluminum species in the nanoparticle core. SAXS data (Figure 1b) indicate that boric acid has no effect on the morphology or size of the nanoparticles formed above the cac. This indicates that boron is in solution after initial silica self-assembly and its main effect is to lower the pH. Additionally, the scattering intensity is greatest from the solution with boron. This could be the result of an increased particle number density, changes in the structure factor, or changes in the scattering length density (SLD). The structure factor does not contribute significantly at length scales associated with intraparticle scattering in dilute systems ($q > \pi/D_{\max}$). Also, the SLD of the particles should be similar because they are formed in solutions of similar compositions. Therefore, different particle number densities are the most probable cause of the increase in scattering intensity. It has been shown that increasing silica concentration above the cac results in a higher number density of particles with a fixed size.[46] In practice, the addition of boric acid lowers the silica solubility (cac) and increases the concentration of nanoparticles.

3.2. Nanoparticle Evolution at 80 °C. Studies of the growth of silica nanoparticles in the presence of boron at 80 °C indicate that boron is not sequestered into the nanoparticles during heating.

The SAXS patterns in the inset of Figure 2 show that the scattering shifts to lower *q*-values and that the scattering intensity increases when the solutions are heated. This indicates that the particle size is increasing (Figure S2a in the Supporting Information), and inversion of the scattering patterns shows that the particles are similar in shape for all the heating times. In Supporting Information Figure S2b the tail of the PDDF at $r > 3$ nm deviates from the analytical PDDF derived for monodisperse spheres[47] indicating that the particles in the solution are polydisperse or elongated.[16,19] These fits show that the nanoparticles' radius increases about 0.75 nm during the first hour of heating (Figure 2). This is about the thickness of one TEA cation.[48] This growth may result from SDA occlusion into the nanoparticles, as was observed in TPA/SiO_2 systems.[9] After the rapid growth of the particles in the first hour of heating, the particles grow at slower rates.

Boron has a negligible effect on the nanoparticle growth (<30 h and 80 °C), and under the conditions of this experiment (high pH) it is anionic. If it were sequestered into the nanoparticle core through condensation reactions with silica the charge density of the nanoparticles would increase and differences in particle structure would result. However, no changes in the particle size or morphology were detected, which implies that boron is a spectator ion (borate) during the time scales of the nanoparticle growth. This could be the result of the thermodynamics governing borate−silica condensation or due to an electrostatic interaction between borate and the surface charge on the nanoparticle (both are negative). The latter would create an electrostatic barrier that borate may not be able to penetrate unless the temperature is increased or the silica nanoparticles have a lower surface potential.[14,16]

3.3. Zeolite *β* Formation from Silica Nanoparticles. We studied the effect of Al and B on the nucleation and growth of zeolite *β* (Table 1) in dilute conditions amenable to SAXS and DLS analysis.[37]

Solutions with aluminum have a higher conductivity (Figure S3 of the Supporting Information) than the corresponding SiO_2 solutions. The addition of aluminum may change the chemical potential of the solids and oligomers so that more silica is sequestered into a condensed phase where it is less likely to participate in acid−base chemistry. During the first 4 days of heating the solution conductivity increases indicating that hydroxide ions are released and that silica connectivity is increasing throughout this period. After 4 days of heating the conductivity remains approximately constant throughout the rest of the synthesis. There are no substantial differences in the conductivity between the samples with or without boron which implies that borate has a negligible effect on the silica condensation kinetics. This is consistent with the ^{11}B NMR spectra (Figure S4 in the Supporting Information) that indicate that borate is present throughout the entire synthesis. It is interesting that in the silicalite-1 synthesis the pH is constant until nucleation when it increases quickly to a plateau after crystallization is finished.[11,49] This difference suggests that silica reorganization in *β* is more gradual than in silicalite-1.

The SAXS patterns (Figure 3a) from solutions Z1 (with Al and B) and Z4 (with no heteroatoms, Table 1) indicate that two populations of particles are formed after heating.[50] Also, there are substantial differences in the character of the

---

(44) Irwin, A. D.; Holmgren, J. S.; Zerda, T. W.; Jonas, J. *J. Non-Cryst. Solids* **1987**, *89* (1−2), 191–205.

(45) Irwin, A. D.; Holmgren, J. S.; Jonas, J. *J. Non-Cryst. Solids* **1988**, *101* (2−3), 249–254.

(46) Fedeyko, J. M.; Egolf-Fox, H.; Fickel, D. W.; Vlachos, D. G.; Lobo, R. F. *Langmuir* **2007**, *23* (8), 4532–4540.

(47) Porod, G. *Acta Phys. Austriaca* **1948**, *2*, 255–292.

(48) Szostak, R. *Molecular Sieves: Principles of Synthesis and Identification*; Blackie Academic & Professional: London, 1998.

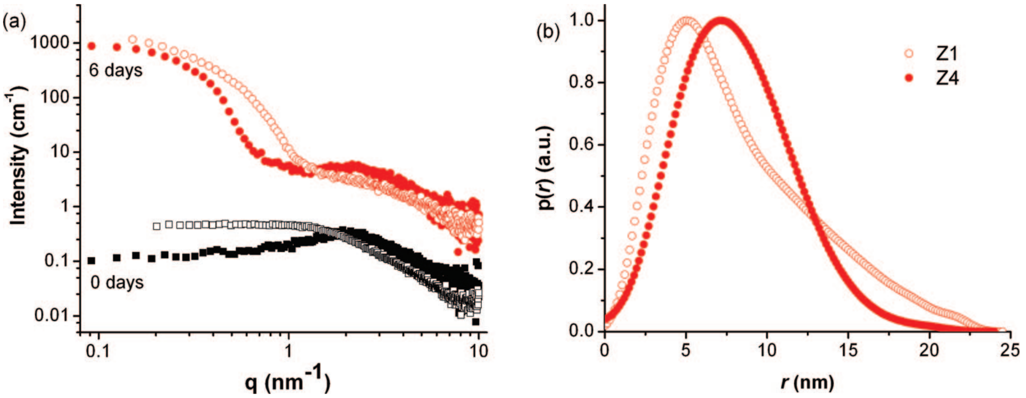

Figure 3. (a) Desmeared SAXS patterns of the solutions Z1 (□, ○) and Z4 (■, ●). Numbers at the left are the hydrothermal synthesis times, and SAXS patterns at 6 days are offset by a factor of 25. (b) PDDFs of the secondary particles after 6 days of hydrothermal synthesis.

particles formed in solutions Z1 and Z4 throughout the hydrothermal synthesis. These differences reflect the minor effect of boric acid and the major effect of aluminum on the nanoparticles formed in these solutions. The silica nanoparticles that self-assemble at room temperature are named primary particles and are <3 nm in diameter for all solutions. Additionally, there is a structure factor contribution to the SAXS patterns from the primary particles formed without aluminum (see the decreasing scattering intensity in the region <2 nm^{-1} from solution Z4 in Figure 3). After heating, a larger population of particles named secondary particles forms. Over time the scattering from the these particles shifts to lower q-values (longer length scales) implying that these particles are growing, whereas the primary particles decrease in number and have an approximately constant size throughout the synthesis. This indicates that the secondary particles are formed from the primary particles.

PDDFs (Figure 3b) indicate that secondary particles with aluminum are elongated or polydisperse. To obtain PDDFs representing the secondary particles the IFT technique was applied over a q-range from about 2 nm^{-1} to the low q-limit. The PDDFs have maxima at 5.0(3) and 7.2(4) nm for solutions Z1 and Z4, respectively. The PDDF of the secondary particles in solution Z4 is close to that of monodisperse spheres with an additional tail at 17.5 nm, whereas the PDDF of the secondary particles in solution Z1 is highly elongated.[51,52] PDDF elongation is evidence of particle polydispersity or elongation, both of which are consistent with aggregation of secondary particles in solutions with aluminum. This is feasible because secondary particles in solutions Z1 and Z2 have a smaller Debye−Hückel screening length relative those in solutions Z3 and Z4 (see the higher electrolyte concentration in Supporting Information Figure S3) resulting in a smaller effective charge which is conducive to particle aggregation.

Scattering from solutions Z1 and Z2 heated for more than 6 days cannot be described adequately by our SAXS data ($D_{\max} < \pi/q_{\min} = 21$ nm).[53] All inversions of SAXS data into real space at these longer times resulted in information that was outside of the limit of resolution for our data. Generally, the tails of the PDDFs from solutions Z1 and Z2 at these times extended to values >30 nm. Therefore, DLS was used to understand the colloidal chemistries at these longer length scales.

DLS studies show that a tertiary population of particles forms in solutions with aluminum after 6 days of synthesis (Figure 4 and Figure S5 in the Supporting Information). The primary particles cannot be detected using this DLS method. After 1 day of hydrothermal synthesis DLS shows that the secondary silica nanoparticles are about 10 nm in diameter. This population in solution Z1 changes for approximately 6 days at which time a tertiary population is observed. No tertiary population is detected in solution Z4. It is notable that the tertiary population's volume percent increases as the secondary population is depleted (Figure S5 in the Supporting Information). A simple explanation for the depletion of the secondary particles is to assume tertiary particles grow via aggregation of secondary particles. Also, the rate of depletion of secondary particles in solution Z2 is greater than in solution Z1. Since the only difference between these solutions is that Z1 contains boric acid, this component must be causing the change in depletion rates. Considering that interparticle forces affect the rates of particle aggregation, those containing boron may have a higher surface charge (higher interparticle electrostatic repulsion) and more steric hindrance to account for the differences in aggregation kinetics. Further studies of these differences will be reported later.

3.4. Separation and Characterization of Tertiary Particles.

The tertiary particles detected using DLS were separated from solution via centrifugation after 14 days of heating. Their size determined by SEM is consistent with DLS, and XRD shows that the tertiary particles are zeolite β (Figure S6 in the Supporting Information). After separating tertiary particles from Z2 at 14 days of heating secondary particles are detected in solution by SAXS and DLS.

An SEM image (Figure 5) of particles extracted from Z1 at 10 days of hydrothermal synthesis shows that the surface

---

(49) Navrotsky, A. *Curr. Opin. Colloid Interface Sci.* **2005**, *10* (5−6), 195–202.

(50) The patterns from Z2 and Z3 are not shown because they are very similar to Z1 and Z4, respectively.

(51) Glatter, O. *J. Appl. Crystallogr.* **1979**, *12* (2), 166–175.

(52) Scattering from secondary particles in Z3 and Z4 fits a Schulz distributed spheres model, and scattering from secondary particles in Z1 and Z2 fits a model for cylinders with Schulz distributed radii.

(53) Feigin, L. A.; Svergun, D. I. *Structure Analysis by Small-Angle X-Ray and Neutron Scattering*; Plenum Press: New York, 1987.

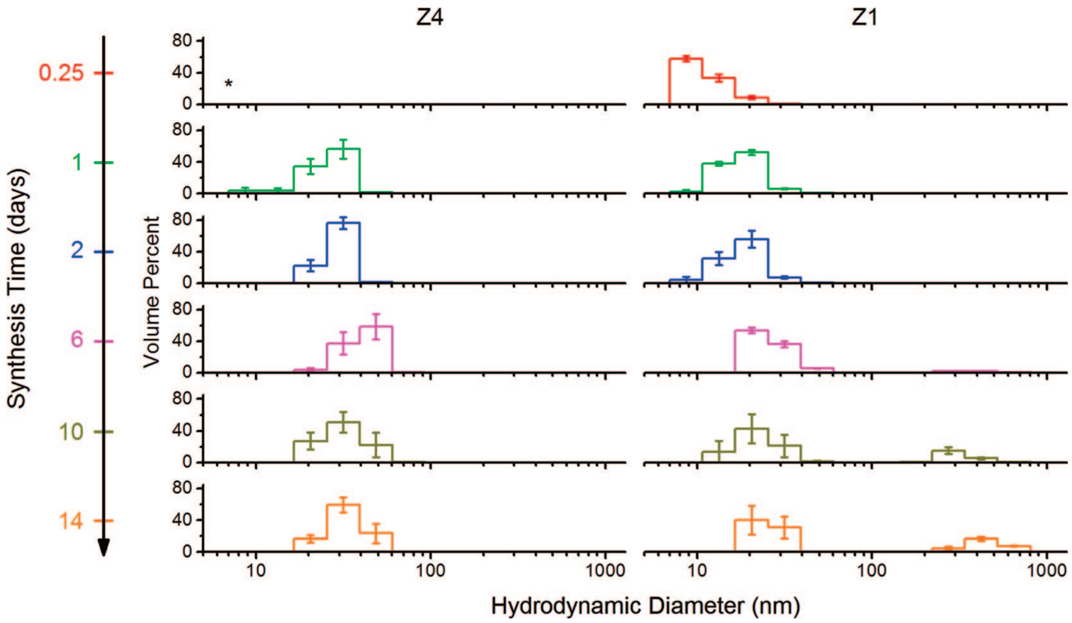

Figure 4. Particle size distributions of the colloids in solutions Z1 (left column) and Z4 calculated from DLS data. Solutions were clarified with 800 nm filters; ∗, data are not available.

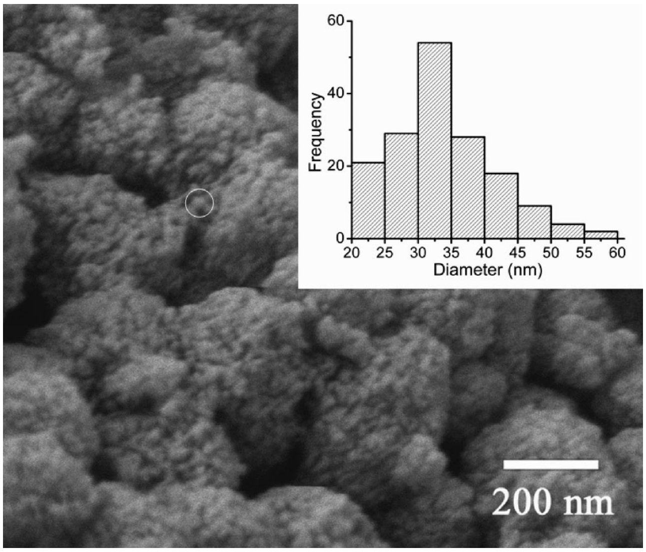

Figure 5. SEM image of particles separated from solution Z1 at 10 days of hydrothermal synthesis. The white circle outlines one of the subunits that make up the particle surface. A particle size distribution (PSD) of the subunits on the surface of the tertiary particles is shown at the inset.

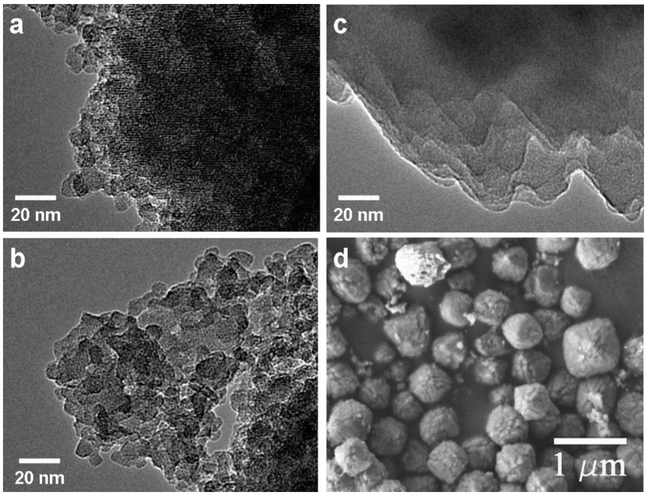

Figure 6. HREM (a and b) images of zeolite β separated from Z1 after 10 days of hydrothermal synthesis. HREM (c) and SEM image (d) of zeolite β crystals separated from Z1 after 28 days of hydrothermal synthesis.

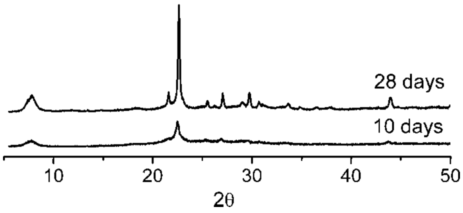

Figure 7. XRD patterns of Z1 after 10 and 28 days of hydrothermal synthesis.

of the particles is composed of units on the order of 30 nm. It is likely that these units are secondary particles that have aggregated into the tertiary particles. Over time the tertiary particle population changes in size, morphology, and crystallinity (Figures 6 and 7). In Figures 6, parts a and b, we see the two ends of the distribution of structure of the tertiary particles. Each tertiary particle appears to be composed of subunits that have regions of low electron density (the pores of zeolite β). However, there are major differences in the ordering of the particles' pores. For example, in Figure 6a only slightly misoriented pores are visible most likely because the secondary particles are aggregating in an oriented fashion similar to what was reported by Davies et al. for silicalite-1.[16] In Figure 6b we see that there is no evident alignment of the pores and that the structure is lacking long-range order. The lack of long-range order of the average zeolite β particle after 10 days of synthesis is evident (due to peak broadness) in the XRD pattern (Figure 7). Quantitative analysis of the long-range order of zeolite β particles using the Scherrer[54] equation and the full width half-maximum of the (302) reflection[55,56] showed that after 10 and 28 days of hydrothermal synthesis the size of the crystalline domains were 26 and 95 nm, respectively. In

Scheme 1

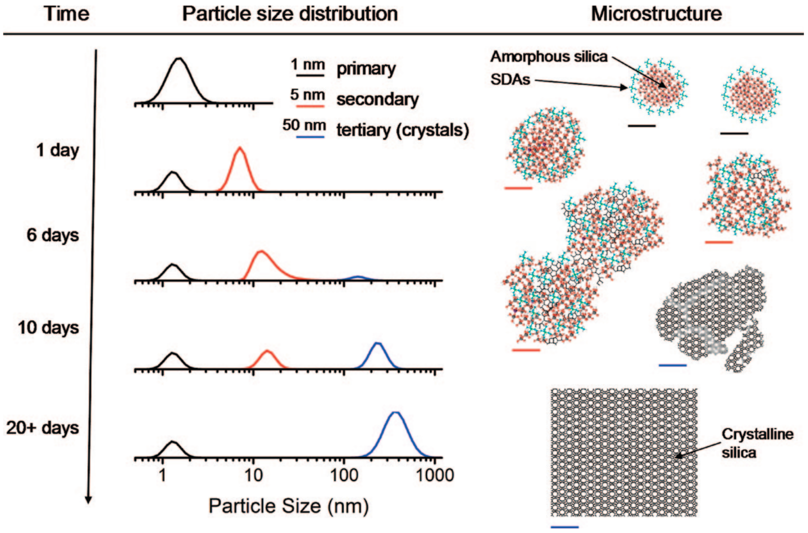

addition, the morphology of the β particles is close to square bipyramidal after 28 days of hydrothermal synthesis (Figure 6d) and the surface of the zeolite β particles becomes smoother (Figure 6c). These findings are consistent with the evolution of the zeolite β particles through solution-mediated silica reorganization.

4. Discussion

4.1. Mechanism of Zeolite β Formation. The results presented here provide the most detailed description of zeolite β formation to date (Scheme 1). The initially clear solutions contain primary particles ($<$3 nm), silicates, aluminosilicates, and borate ions at room temperature. Aluminum has a high affinity for bonding to silicates,[46] whereas boron does not;[44,45] therefore, aluminum and not boron is not sequestered into the primary particles. These primary particles are present throughout the entire synthesis of zeolite β, and their initial concentration is governed by the solubility of silica. The presence of primary particles of this size has been reported by de Moor et al. in the formation of all silica zeolite β from solutions with a H_2O/SiO_2 ratio of 35 and trimethylene-bis(*N*-benzyl, *N*-methyl-piperidinium) SDA.[24] At elevated temperatures, the silicates in solution condense into secondary nanoparticles initially about 6 nm diameter and the conductivity (and pH) of the solution increases simultaneously. Over time the secondary particles grow larger (6−50 nm) by solution-mediated silica rearrangement or by aggregation with primary or other secondary particles.

After 6 days of heating, tertiary particles, identified as zeolite β by XRD, are formed in the solutions containing aluminum. We have shown here that the tertiary particles are aggregates of the secondary particles based on SEM and TEM images that show that the tertiary particles are made up of units similar in size to those of the secondary particles. DLS data also show that the tertiary particles increase in number as the secondary particles are depleted. All of the subunits comprising the tertiary particles observed here were internally well-ordered indicating that β structure evolves within the secondary particles in solution. However, not all secondary particles are well-ordered at 6 days of heating, and therefore, the more ordered ones must aggregate preferentially. A model based on a similar mechanism for silicalite-1 growth was reported by Drews and Tsapatsis.[19]

It seems that there is a distribution of internal structure in the secondary particles and that there is an inverse correlation between their degree of structural order and the magnitude of their surface charge and potential. Provided that electrostatic forces are the main barrier to particle aggregation this postulate leads to the conclusion that only secondary particles having zeolite β structure aggregate into tertiary particles. The relationship between the surface charge and the internal structure of the secondary particles follows an earlier report[13,15,57] that determined that precursor particles initially have a core−shell structure with the core composed of silica and the shell composed of SDAs. In this state the particles have the highest surface charge and repel each other as evidenced by their stability in solution. After heating, the cationic SDAs migrate (balanced by a silyl group) inside of the nanoparticle and the surface charge decreases. It is not clear whether the secondary particles have a core−shell structure, but the occlusion of SDAs results in formation of a zeolite β-like microstructure (high framework connectivity), charge balance within the secondary particles, and a decrease of the secondary particles' surface charge.

Once the tertiary particles have formed they have a distribution of internal order. In Figure 6, parts a and b, we see that some of the crystals have long-range order, whereas others are highly disordered. This is evidence that some of the secondary particles aggregate oriented with the crystal domain of the tertiary particles, similar to the model proposed by Davis et al.,[16] but others aggregate in random orientations. This mechanism of aggregation gives rise to a distribution of internal organization in the tertiary population. The

---

(54) Warren, B. E. *X-Ray Diffraction*; Dover: New York, 1990.

(55) Higgins, J. B.; LaPierre, R. B.; Schlenker, J. L.; Rohrman, A. C.; Wood, J. D.; Kerr, G. T.; Rohrbaugh, W. J. *Zeolites* **1988**, *8* (6), 446–452.

(56) Treacy, M. M. J.; Newsam, J. M. *Nature* **1988**, *332* (6161), 249–251.

(57) Rimer, J. D.; Vlachos, D. G.; Lobo, R. F. *J. Phys. Chem. B* **2005**, *109* (26), 12762–12771.

aggregation of secondary particles into tertiary particles could have an impact in the design of hierarchically ordered materials. For instance, once the secondary particles obtain the structure of zeolite β, surfactants can be added into the solution to aggregate the secondary particles into microporous−mesoporous hybrid materials.[33,58,59]

We also observed a change in the surface texture of the tertiary particles from rough (10 days) to smooth (28 days). This cannot be accounted for solely by addition of secondary nanoparticles to the growing zeolite crystal, because these particles are at least 5 nm in diameter, or by internal reorganization of silica, which is unlikely to effect external structure. The smoothing may proceed by dissolution of less ordered silica domains from the tertiary particles (such as rough surfaces and regions of misoriented secondary particles) and by redeposition of monomers and small oligomers onto the surface of tertiary particles, a mechanism named solution-mediated silica reorganization.[60]

Mintova et al. have successfully synthesized zeolite β nanocrystals in more concentrated solutions (H_2O/SiO_2 11.8) using TEAOH as the SDA.[32] They reported that the precursor particles are initially about 10 nm in diameter and that they do not exhibit zeolite β microstructure. These particles detected by Mintova et al. may be similar to the secondary particles initially formed after heating solutions Z1 to Z4. It is noteworthy that Mintova et al. did not report the formation of a primary population of particles (<3 nm). This may be because DLS, used by Mintova et al., is less sensitive to small particles than SAXS is. Indeed we could not detect the primary particles using our DLS setup. They also observed a direct correlation between the rate of zeolite β formation and aluminum concentration in the synthesis solution. In our synthesis aluminum was a requisite for the formation of tertiary particles. However, other trivalent elements such as boron decreased the crystal growth rate for zeolite β. This indicates that boron may be incorporated into the secondary particle surface resulting in increased particle surface charge and stability. It is also interesting that Mintova et al. prepared all-silica zeolite β. This suggests that the secondary particles in solutions Z3 and Z4 may be crystalline even though we were unable to separate them from the solution by centrifugation. Mintova et al. may have been able to precipitate these particles because their synthesis was carried out at a silica concentration that was about 7 times greater than that studied here.

The XRD data from the particles synthesized by Mintova et al.[32] (see their Figure 2) shows that they are not as well-ordered as the tertiary particles formed in Z1 after 28 days of hydrothermal synthesis (Figure 7). This difference in crystalline character may also result in differences in the thermal stability of the particles. The particles that Mintova et al. showed to be zeolite β by XRD are aggregates of 30−50 nm particles which is consistent with our proposal that some of the secondary particles in Z1 and Z2 have zeolite β microstructure.

4.2. Comparison to Silicalite-1 Formation Mechanism. The mechanism for silicalite-1 formation from dilute solutions[8,9,12,13,16,19,57,61] is compared to the proposed zeolite β formation mechanism to search for a general mechanism of zeolite formation.

In clear solutions of TEOS and TPAOH silica self-assembles into small colloidal nanoparticles (<5 nm)[13] that are stable at room temperature due to electrostatic and steric forces that result from their anionic silica core and cationic SDA shell.[9,16] NMR data provide evidence that the silica present in the PNs is primarily in the Q^3 configuration and that the coordination is affected by the TPAOH concentration.[62] With the use of ATR/FTIR Patis et al. showed that the PNs did not have the structure of silicalite-1 (see their Figure 3).[12] Additionally, modeling of the PNs shows that they are amorphous during the initial stages of silicalite-1 formation.[63] The characteristics of these precursor particles formed above the cac are similar to the primary particles in our mechanism for zeolite β formation.

At elevated temperatures or longer time scales the TPA−silica nanoparticles no longer exhibit a well-defined core−shell structure.[16,57] This indicates that the SDAs are embedding into the nanoparticle core and marks the onset of ordering that gives rise to more zeolite-like materials referred to as “intermediate” particles.[19] These changes have been detected by ATR/FTIR[12] and NMR.[8,17] In the synthesis of zeolite β it is interesting that changes in the size of the primary particles are not detected by SAXS (at times >2 days). In each case the secondary particles (in zeolite β) and intermediate particles (in silicalite-1) are formed from the primary population of particles. However, the details of secondary particle formation have not been elucidated. The intermediate TPA−silica nanoparticles grow by Ostwald ripening.[10,57] After an induction period (>30 days at 293 K) the most ordered intermediate particles serve as silicalite-1 nuclei.[16] It is probable that the most ordered secondary particles serve as the zeolite β nuclei as well since some secondary particles have zeolite β structure (by HREM). After nucleation when the secondary particles (β) and intermediate particles (silicalite-1) are about 6−50 and 5 nm,[16] respectively, they aggregate selectively into a tertiary particle population. The selectivity depends on the stability of the secondary (or intermediate) particle population, and the observation that the tertiary particles are composed of secondary units with high internal order indicates that these particles are those that have the least colloidal stability.

Several mechanisms for silicalite-1 growth ranging from solution-mediated silica reorganization[64] to oriented aggregation of nanoparticles have been proposed.[16,18,19] In this report the dominant mechanism of tertiary particle growth was

---

(58) Zhang, Z.; Han, Y.; Zhu, L.; Wang, R.; Yu, Y.; Qiu, S.; Zhao, D.; Xiao, F.-S. *Angew. Chem., Int. Ed.* **2001**, *40* (7), 1258–1262.

(59) Perez-Pariente, J.; Diaz, I.; Agundez, J. *C. R. Chim.* **2005**, *8* (3−4), 569–578.

(60) Cundy, C. S.; Cox, P. A. *Microporous Mesoporous Mater.* **2005**, *82* (1−2), 1–78.

(61) Kumar, S.; Davis, T. M.; Ramanan, H.; Penn, R. L.; Tsapatsis, M. *J. Phys. Chem. B* **2007**, *111* (13), 3398–3403.

(62) Aerts, A.; Follens, L. R. A.; Haouas, M.; Caremans, T. P.; Delsuc, M. A.; Loppinet, B.; Vermant, J.; Goderis, B.; Taulelle, F.; Martens, J. A.; Kirschhock, C. E. A. *Chem. Mater.* **2007**, *19* (14), 3448–3454.

(63) Auerbach, S. M.; Ford, M. H.; Monson, P. A. *Curr. Opin. Colloid Interface Sci.* **2005**, *10* (5−6), 220–225.

(64) Schoeman, B. J. *Microporous Mesoporous Mater.* **1998**, *22* (1−3), 9–22.

observed to change from particle aggregation initially after nucleation to solution-mediated silica reorganization later in the synthesis. The key to this discovery was observing the evolution of the surface texture, morphology, and crystallinity (by XRD) of the tertiary particles. This suggests that by investigating the silicalite-1 crystal surface over time the discrepancies between the two presented mechanisms of silicalite-1 growth may be resolved. In general, each of these mechanisms of formation may be dominant at different synthesis times (or crystal particle sizes),[60] and the most accurate description of zeolite growth may be a combination of them. These results are promising because they indicate that it is possible to develop a mechanism consistent with the formation of different zeolites in clear solutions.

5. Conclusions

Investigation of silica nanoparticles shows that boric acid is a spectator ion in the self-assembly of silica in aqueous solutions of TEA. In effect, boric acid decreases the pH of the solution and the solubility of silica resulting in the formation of a greater number of nanoparticles of a fixed size. Upon heating the nanoparticles at 80 °C they grow to larger sizes similar to that for systems containing TPA and silica. Borate was observed to be a spectator ion the evolution of the size and morphology of the nanoparticles for all times studied (<30 h).

In the synthesis of zeolite *β* three populations of particles are detected in solution. Primary particles (<3 nm) are formed at room temperature above the cac, and upon heating, the number of these primary particles decreases and secondary particles are observed in solution (6−50 nm). In solutions that contain aluminum the secondary particles aggregate into tertiary particles (zeolite *β*, < 200 nm) that are not stable in solution. The observation that secondary particles aggregate into zeolite *β* can be used to develop new strategies for synthesis of materials with enhanced long-range order. For instance, it may be possible to tune the rate of secondary particle aggregation to improve alignment at the interface between the growing zeolite crystal and the secondary particle. Before these strategies are employed the forces that affect secondary particle aggregation must be understood. In this report we propose that there is an indirect relationship between the microstructure and the stability of the particles in solution to account for the induction time for secondary particle aggregation and zeolite *β* nucleation.

Initially the structure of the tertiary particles is dominated by aggregation of secondary particles as evidenced by their poor crystal structure, rough surface, and oblate morphology. At later times in the synthesis they evolve into zeolite *β* crystals with long-range order and smooth square bipyramidal morphology by solution-mediated silica reorganization. These observations indicate that the dominant mechanism of zeolite growth changes with synthesis time (or crystal particle size).

Acknowledgment. The authors acknowledge Dr. S. Bai for help with NMR data collection and processing and W. Pyrz for collection of HREM images. R.F.L. thanks the National Science Foundation for financial support under Grant CBET-0522435 and the National Institute for Standard and Technology for financial support under Grant No. 70NANB7H6178.

Supporting Information Available: pH data collected in cac studies, PDDFs from the evolution of silica particles at 80 °C and monodisperse sphere fits, conductivity measurements from the zeolite *β* syntheses, solution NMR data at selected times from the zeolite *β* syntheses, time-resolved DLS data collected from Z2, evidence of zeolite *β* separation from synthesis solutions (PDF). This material is available free of charge via the Internet at http://pubs.acs.org.

CM800884Q